Low Reynolds Number Flow Dynamics and Control of a Pitching Airfoil with Elastically Mounted Flap Actuator

Final Report by

Sourabh V. Apte

School of Mechanical Industrial Manufacturing Engineering

Oregon State University

ASEE Summer Faculty Fellowship Program

Wright-Patterson Airforce Base

June 19-August 26 2011

AFRL Research Advisor and Sponsor: Dr. Miguel Visbal

Acknowledgement

Support through ASEE's Summer Faculty Fellowship Program is greatly appreciated. Interactions and discussions with Dr. Miguel Visbal were critical for the direction of this exploratory research, specifically looking at trailing edge flap in a flapping wing configuration. Interactions with researchers at the Computational Sciences Division of Wright Patterson Airfoil Base and Dr. Justin Jaworski (presently at University of Cambridge) are also acknowledged. Computations were performed on Lonestar machine at the Texas Advanced Computing Center.

Abstract

Direct numerical simulations were performed to study the effect of an elastically mounted leading and trailing edge flap on the unsteady flow over a flat, thin airfoil at Reynolds number of 14700 based on the chord length. The goal is to investigate potential benefits of flow-induced passive actuation of the leading or trailing edge to the lift and drag characteristics of MAV foils. The flap, attached with a torsion spring at one-third the chord length, is modeled as a spring-mounted compound pendulum. It may undergo flow induced rotation resulting in dynamic variations in the effective angle of attack as well as the airfoil shape. Firstly, the second-order, fictitious domain based finite volume approach by Apte *et al.* (J. Comp. Phys. 2009) was extended to model this fluid-structure interaction problem on a fixed, Cartesian mesh. Verification studies were conducted on a canonical test case of a spring-mounted cylinder to show good predictive capability. Secondly, for the leading edge actuator, computations were performed at 20° angle of attack and varying the spring parameters. A lock-in region leading to limit cycle oscillations of the leading edge flap was obtained that resulted in improvements to lift-to-drag ratios. Finally, flow over a plunging airfoil (representative of flapping wing flight), at reduced frequency of 5.71 (10 Hz) and 5° angle of attack was investigated with and without the flapping actuator near the trailing edge. It was found that, spring natural frequencies higher than the plunging frequency result in the flap actuation leading to net increase in thrust. This preliminary work suggests that a simple flap actuator may be used to provide passive (or active) control for better performance of MAVs. The summer research at AFRL's computational sciences division has resulted in several opportunities for future collaborations with AFRL scientists and researchers. At Oregon State, new projects for senior students are initiated to build and modify the existing physical setup and measure lift and drag coefficients. A test rig for wind-tunnel experiments with simultaneous plunging of the airfoil and flapping of the airfoil together with torsion-spring mounted leading or trailing edge is being built. The work is also being presented at American Physical Society's November Meeting (Baltimore) and will be submitted to the AIAA fluid dynamics conference.

1 Introduction and Objectives

The desire to advance the use of thin, low Re wings at small scales introduces flow dynamics that significantly influence their performance and flow control. At sufficiently high angles of attack during transients, flow over an airfoil separates, which can lead to a 'dynamic stall' condition. One major concern of thin airfoil design, when operating at high lift conditions, is the unsteady nature of separation at the leading edge resulting in a Kelvin-Helmhotlz type flow instability [1, 2, 3]. This causes the generation and convection of low frequency large vortical structures that have a strong influence on unsteady lift. Very early works on flow over hydrofoils and wings [4, 5] have shown a strong correlation of pressure in the separation bubble with the onset of stall conditions.

At low Re, thin flat airfoils actually *delay* stall to higher angles of attack when operating at lower aspect ratios, although the lift is somewhat lower at lower angles of attack [6]. It has been shown that a cambered plate (4%) performs better in the Re range of 10^4–10^5 [6], and has a low sensitivity to the trailing edge geometry and the turbulence intensities [7]. Although thin airfoils show many advantages at low Re, such as high lift-to-drag ratio, they exhibit *wide fluctuations in lift* mainly caused by the unsteady flow separation at the leading edge [8]. The character of this separation is highly unsteady, at fairly low frequencies, and generally without reattachment if the angle of attack is sufficiently large [8], however, most of this work is at somewhat higher Re ($\sim 3 \times 10^5$).

Extensive studies at low Re have been carried out to better understand the flow and its dynamic characteristics for stability and control considerations. For very low Reynolds number [$\mathcal{O}(100)$], the unsteady flow characteristics of thin wings undergoing plunge maneuvers show downstream advection of the leading edge vortex and the frequency for unsteady lift characteristics [9]. Other studies of unsteady flow characteristics during pitching include [10, 11, 12, 13] and recent computational work based on immersed boundary technique under the AFOSR MURI program at CalTech on impulsively started wing [14, 15, 16]. It is clear from these and other studies that vortex shedding, advection, and strength is highly dependent on the maneuvering characteristics. Recent numerical studies at AFRL by Visbal and co-workers [17, 18] on low Re plunging airfoils have indicated that plunging motion significantly alters the dynamic stall vortex by breaking down the vortex as it plunges against the airfoil surface. High-frequency small-amplitude plunging oscillations of stalled airfoil resulted in elimination of coherent vortex structures propagating along the airfoil surface.

There is considerable interest in biologically inspired flows with applications to **micro-air vehicles with flapping wings** and small unmanned vehicles [19, 20, 21, 22, 23]. AFOSR has renewed interest in designing efficient and stable MAVs with flapping wings that are easily maneuverable and resistant to flow disturbances. Considerable effort has been devoted to looking at flexible wings, following the bird flight such as bats, for

such designs. However, providing fundamental analysis explaining resultant increase in propulsion efficiency or thrust owing to flexibility has been a challenge due to the complexity of the fluid-structure interaction problem.

Last year as part of the ASEE SFFP work [24], effect of forced oscillatory sinusoidal oscillations of the leading edge actuator (see Figure 1, top panel) on the flow dynamics and lift-to-drag ratio was investigated in detail using DNS [24, 25, 26]. The airfoil studied was a thin, flat (thickness-to-chord ratio of 0.02) with high aspect ratio ($AR = 2.56$)] at $Re = 14700$ and at an angle of attack (α_0) of 20°. Use of *static actuation* [that is, altering the effective angle of attack by setting the leading edge actuator angle $\theta = 20°$ (leading edge parallel to the flow)] or *dynamic actuation* [that is, oscillatory flapping of leading edge], the mean lift-to-drag ratio was increased [24, 25, 26]. It was found that at high frequencies (reduced frequency, $k \geq 5.7$), oscillatory actuation of the leading edge resulted in significant increase in mean lift-to-drag ratio. With lower amplitudes of dynamic actuation, the fluctuations in lift and drag coefficients were also small and predictable [24]. Forced oscillations at frequencies that match the actuation time scale ($1/f$) to the convective time scale of traveling leading edge vortices (ℓ_a/U_∞) created pair of counter-rotating leading edge vortices that break down near the hinge, resulting in smaller wake and reduced drag.

Based on the established practices in developing control strategies [27], an important extension of this prior work was proposed that involves use of a **passive control study** to better understand the flow dynamics and flow-actuator interactions. Accordingly, it was proposed to investigate effects of flow induced actuation on the lift and drag characteristics at high angles of attack under steady flow as well as unsteady pitching maneuvers. The **central hypotheses** for the proposed work are:

(i) *flow-induced activation* of the leading (or trailing) edge actuator and resultant open loop control provides an effective mechanism to alter leading-edge vortex shedding, separation-bubble dynamics, and dynamic stall conditions;

(ii) appropriate design of the torsion spring

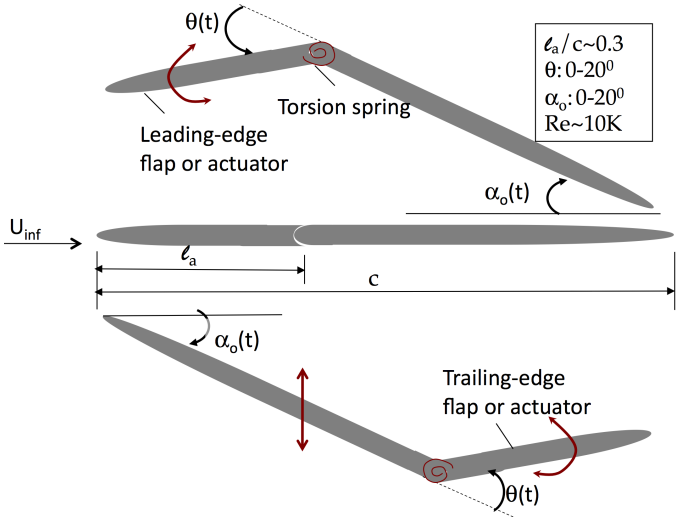

Figure 1: Schematic of a thin, flat airfoil with a torsion spring mounted leading or trailing edge actuator. A typical flap, length (ℓ_a) approximately 30% of the chord (c), will be hinged to the airfoil body to facilitate change in flap angles (θ). The foil may undergo plunging motion to represent flapping wing mechanism, however, the angle of attack α_0 is kept constant.

may result in flow-induced limit cycle oscillations of the leading (or trailing) edge flap and enhance lift-to-drag ratios and performance;

(iii) use of a trailing edge spring-mounted actuator, combined with plunging motion of the airfoil (representative of flapping wing mechanism), may result in increased thrust and propulsion efficiency for certain range of spring flexibility.

The following research objectives were devised to test the above hypotheses and investigate the flow-structure interactions and resultant performance benefits for thin, flat airfoils.

I. Verify the fictitious domain immersed boundary approach for flow-induced actuation of the leading (or trailing) edge flap. Extend the fictitious domain method developed by Apte *et al* [28], to account for flow-induced oscillations of the flap actuator with one-degree of freedom (rotation around the hinged point).

II. Quantify the effect of flow-induced dynamic changes in the leading or trailing edge flap actuation on the aerodynamic loads and performance.

The results for these main objectives are summarized below.

2 Methodology:

The computational algorithm for flow over immersed objects on simple Cartesian grids is based on a fictitious domain approach [28, 29]. In this approach, the entire fluid-rigid body domain is assumed to be an incompressible, but variable density, fluid. The flow inside the fluid region is constrained to be divergence-free for an incompressible fluid, whereas the flow inside the particle (or rigid body) domain is constrained to undergo rigid body motion (i.e. involving translation and rotational motions only). For specified motion of the rigid body, the rigidity constraint force can be readily obtained once the location of the boundary of the rigid body is identified by making use of marker points in a banded region surrounding the rigid body surface. The marker points provide subgrid scale resolution, improving the accuracy of interpolations between the marker points and the background grid. Due to rigidity of the moving object, there is no relative motion between the marker points, and all points move with the same, specified velocity field.

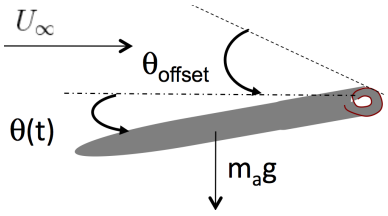

Figure 2: Torsion spring dynamics modeled as a spring mounted compound pendulum.

Using the torque due to gravitational and aerodynamic forces as well as considering pre-tension in the torsion spring, the following non-dimensionalized dynamic equation based on spring-mounted compound pendulum can be derived. It is assumed that, the mean position of the front-flap is with an offset flap angle equal to the angle of attack; $\theta_{\text{offset}} = \alpha_0$ resulting in a horizontal front flap in the mean. This results in a

non-linear equation (due to the gravitational torque):

$$\frac{d^2\theta}{d\tau^2} + 4\pi\xi St_{\mathrm{N}}\frac{d\theta}{d\tau} + \left(2\pi St_{\mathrm{N}}\right)^2\theta + \frac{3}{2}\left(\frac{g\ell_a}{U_\infty^2}\right)(1-\cos\theta) \quad = \quad \frac{3}{2}\left(\frac{\ell_a}{t_a}\right)\frac{C_M}{\mathcal{I}^*}, \tag{1}$$

where $\mathcal{I}^* = \mathcal{I}/(m_f\ell_a^3/3) = \rho_a/\rho_f$ is the moment-of-inertia ratio (ratio of moment of inertia of the actuator about the hinged point to the moment of inertia of the equivalent fluid) which turns out to be the ratio of the actuator density to the fluid density, $\tau = tU_\infty/\ell_a$ is the non-dimensional time, $St_{\mathrm{N}} = f_{\mathrm{N}}\ell_a/U_\infty$ is the Strouhal number based on the natural frequency of the spring ($f_{\mathrm{N}} = \frac{1}{2\pi}\sqrt{K/\mathcal{I}}$), K is the spring stiffness parameter, C is the damping coefficient, $\xi = \frac{C}{2\sqrt{K\mathcal{I}}}$ is the non-dimensionalized damping parameter, g is the gravitational acceleration, θ is the actuator angle (positive anti-clockwise), ℓ_a is the actuator length, t_a is the airfoil thickness, and C_M is the net pitching moment around the hinge based on the torque acting on the actuator.

In the above equation, the gravitational term was found to have small effect on the spring dynamics compared to the other terms. At zero angle of attack, if the actuator is in the front, the drag and lift forces produce torques that tend to move the actuator away from its desired mean position (increasing θ) and thus are destabilizing. Whereas with a tail actuator, the drag and lift forces tend to move the actuator toward the desired mean position of $\theta = 0$.

The above equation is solved by decomposing it into two coupled first-order ODEs and using an explicit third-order Runge-Kutta scheme. The pitching moments are obtained from the fluid flow solver and a new angular velocity and position for the actuator are determined. In order to incorporate fluid-structure interaction problem of a torsion-spring mounted front or tail flap, the basic algorithm was modified. The torsional spring dynamics equations were first obtained by using a spring-mounted compound pendulum formulation. The solution to the spring dynamics equation was linked to the flow field solution using an iterative method, wherein the Navier-Stokes equations and the spring equations are solved multiple times with better approximation for the unknown flap displacement and motion within each time-step. The coupled algorithm was verified together with grid convergence study for a spring-mounted cylinder case and solutions compared against published data. The flow solver is fully parallel and based on conservative finite volume scheme [30] for accurate prediction of turbulent flows.

3 Results

The above formulation was applied to investigate the effectiveness of a passive flap actuator with the flap in the leading or trailing edge. First the approach and numerical scheme was verified by investigating flow over a spring-mounted cylinder and comparing the numerical predictions against published data.

3.1 Verification Tests

Flow over spring-mounted cylinder with two-degrees of freedom has been studied extensively as a canonical test case for fluid-structure interaction problem [31, 32, 33, 34]. The motion of the cylinder center (x_a, y_a) due to this fluid-structure coupling is governed by the following non-dimensionalized equations:

$$\frac{d^2x_a}{dt^2} + 4\pi\xi St_{\mathrm{N}}\frac{dx_a}{dt} + (2\pi St_{\mathrm{N}})^2 x_a = \frac{2}{\pi m^*}C_D \tag{2}$$

$$\frac{d^2y_a}{dt^2} + 4\pi\xi St_{\mathrm{N}}\frac{dy_a}{dt} + (2\pi St_{\mathrm{N}})^2 y_a = \frac{2}{\pi m^*}C_L, \tag{3}$$

where $f_{\mathrm{N}} = f_{\mathrm{N}x,y} = \frac{1}{2\pi}\sqrt{(K_{x,y}/m)}$, $St_{\mathrm{N}} = \frac{f_{\mathrm{N}}D}{U_\infty}$, $\xi = \xi_{x,y} = \frac{C_{x,y}}{2\sqrt{mK_{x,y}}}$, $m^* = m_c/m_f = m_c/(\pi/4\rho_f D^2)$, m_c is the cylinder mass, D is the cylinder diameter, and C_D, C_L are the drag and lift coefficients, respectively.

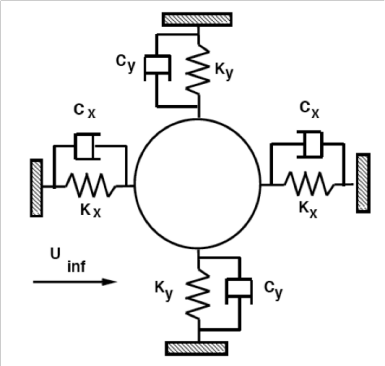

Figure 3: Spring mounted cylinder with two-degrees of freedom.

For flow over cylinder at $Re = 200$, the computational domain chosen was 30 times larger than the cylinder diameter in the x and y directions. Two grid cells were used in the spanwise direction with periodic boundary conditions. A uniform Cartesian grid was used around the cylinder center in a small patch to have well-resolved cylinder surface. The grid was stretched away from the cylinder. Three grid resolutions were used around the cylinder: $D/33$ (coarse), $D/66$ (medium) and $D/83$ (fine). Time step used is 2.5×10^{-3}, giving a cfl number of around 0.2. First, flow over a rigid cylinder at $Re = 200$ was computed providing vortex shedding with a Strouhal number, $St = 0.1986$. The natural frequency of the spring was set based on this vortex shedding frequency by using $St_{\mathrm{N}} = St$.

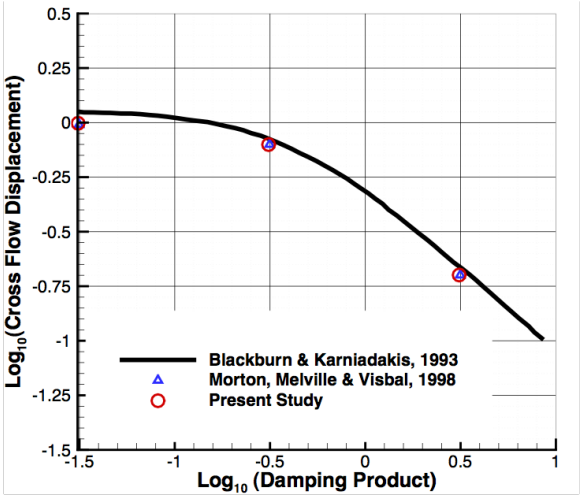

Figure 4: Cross-stream displacement for different damping coefficients compared to published data.

Multiple inner iterations per time-step were used to solve the fluid-structure interaction problem. It was found that, 3 and 5 inner iterations provided virtually identical solutions. With no inner iterations, the solution significantly over-predicted the cross-stream displacement of the cylinder. In all future simulations, three inner iterations were used. Figure 4 shows comparison of the cross-stream displacement of the cylinder center with other approaches based on spectral predictions by Blackburn & Karniadakis [32] and body-fitted, deforming grid algorithm of Morton *et al* [31] for different damping coefficients. Excellent prediction

is obtained using the present scheme. Other statistics such as variations in drag and lift coefficients we also predicted well compared to these studies [34].

3.2 Flow Over Thin Flat Airfoil with Passively Actuated Front Flap

Flow over a thin, flat airfoil at $Re = 14700$ and an angle of attack (α) of 20° is investigated. The chord length (c) is 20 cm, the thickness to chord ratio is 0.02, and the actuator length (ℓ_a) to chord ratio is 0.3. The airfoil has elliptical rounded edges with a ratio of 5:1. Grid resolutions used in the present calculations are given in figure 5. The baseline resolution is finer than that used for corresponding studies on the plunging SD7003 performed last year as part of the ASEE work [25, 26] that showed good predictive capability in comparison to AFRL's FDL3DI solver [17].

Grid	$\Delta x/c$	$\Delta y/c$	$\Delta t U_\infty/c$
Baseline	0.00166	0.00166	0.000125
Coarse (Non-Uniform)	0.005	0.00166	0.00025

Figure 5: Cartesian grid resolution for thin, flat airfoil studies.

In order to investigate the effect of passively actuated leading edge flap, a baseline case of 20° angle of attack ($\alpha_0 = 20°$) is considered. For the passively actuated front flap, the mean actuator angle is intended to be equal to the angle of attack ($\theta = \alpha_0$), making the flap horizontal in the mean. In order to get strong coupling, the moment of inertial ratio $\mathcal{I}^*$ and the spring stiffness (or natural frequency/Strouhal number, St_N) were varied. The damping coefficient (xi) was held constant at 0.05. Four moment of inertia ratios were investigated: $\mathcal{I}^* = 42,\ 52.5,\ 84,\ 1000$. Increase in $\mathcal{I}^*$ results in decreased motion of the flap (owing to increased weight), with $\mathcal{I}^* \to \infty$ being very inertial. In addition, the spring stiffness was varied to obtain natural frequencies of $f_\mathrm{N} = 10,\ 5\ ,3$ Hz. Even for low moment of inertia ratios, most oscillations in the actuator position were observed for the spring natural frequency of 3 Hz, suggesting a lock-in region around this frequency. For higher frequencies studied, the variations in the actuator angle (θ) were very small.

Figures 6a,b show temporal variation of lift and drag coefficients (based on forces acting on the actuator only) and resultant actuator angle variation during passive actuation of the front flap. The angle of attack is held fixed at 20° and the spring constants are chosen with natural frequency of $f_\mathrm{N} = 3$ Hz and damping coefficient of $\xi = 0.05$. The pretension in the spring is set such that the mean position of the front flap is at $\theta = 20°$. It is observed that with smaller moment-of-inertia ratio $\mathcal{I}^* = 42.6$, large periodic variations in the flap angle are obtained that are dictated by similar variations in lift and drag coefficients on the actuator. This type of periodic oscillation of the front flap was not observed if the spring stiffness is higher providing higher natural frequencies. This suggests that a lock-in behavior is obtained for spring natural frequency of around $f_\mathrm{N} = 3$ Hz. This also suggest a time-scale of around 0.33 s for the leading edge vortex formation. Similar, periodic oscillation is observed for twice the moment-of-inertia ratio $\mathcal{I}^* = 85.2$, although the amplitude of actuator angle variation is reduced owing to heavier flap.

Figure 6c shows the effect of passive actuation of the leading edge on the overall airfoil lift-to-drag ratio.

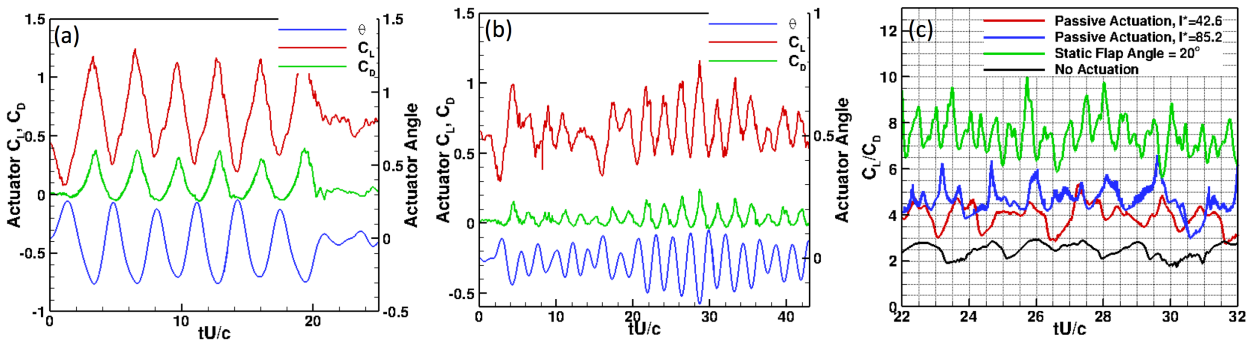

Figure 6: Effect of passive actuation of the leading edge flap for $\alpha = 20°$, $Re = 14700$ with the mean flap angle of $\theta = 20°$ and spring natural frequency of $f_N = 3$ Hz: (a) Actuator C_L, C_D and displacement θ for $\mathcal{I}^* = 42.6$, (b) Actuator C_L, C_D and displacement θ for $\mathcal{I}^* = 85.2$, (c) Airfoil lift-to-drag ratio C_L/C_D for varying rigidity of the flap.

With no actuation, at 20° angle of attack, the lift to drag ratio varies between 2 and 3. However, with a spring mounted flap, the lift-to-drag ratio is increased suggesting that passive actuation indeed results in increased performance. With increasing weight of the actuator (increase in $\mathcal{I}^*$), the gain in lift-to-drag ratio is higher. This can be explained as follows. With lower $\mathcal{I}^*$, the actuator undergoes large displacements around its mean position of $\theta = 20°$. This results in shedding of larger leading vortices and larger wake regions, increasing the drag on the airfoil. With increase in $\mathcal{I}^*$, the magnitude of actuator angle variation is reduced. With very high value of $\mathcal{I}^* = 1000$, the actuator remains nearly static and provides the most benefit in increasing lift-to-drag ratio. Table 1 summarizes the variation in lift and drag coefficients on the wing for varying inertia-ratios. It indicates that, with passive actuation, the drag coefficient is reduced substantially whereas the reduction in lift coefficient is not as significant compared to no actuation case. It also indicates that, with increase in inertia ratio, the lift coefficient slightly increases and the drag coefficient decreases owing to small oscillations in front actuator. For very large inertia ratio (almost static actuation), the drag coefficient is much smaller, however the lift coefficient is also reduced. The overall lift-to-drag ratio for static actuator is much larger compared to no actuation.

Table 1: Passive actuation of leading edge at $\alpha_0 = 20°$, $Re_c = 14700$, $\mathrm{St_N} = \mathrm{f_N}\ell_\mathrm{a}/\mathrm{U}_\infty = 0.16$, $\xi = 0.05$.

Actuation	$\mathcal{I}^*$	C_D	C_L	C_L/C_D
None	-	0.68	1.62	2.39
Passive	42	0.359	1.433	3.99
Passive	52.5	0.355	1.44	4.06
Passive	84	0.347	1.46	4.2
Passive	1000(static)	0.2	1.33	6.65

3.3 Flow Over Thin Flat Airfoil with Passively Actuated Tail Flap

An exploratory simulation for flow over a wing held fixed at 0° and 10° angles of attack with passively actuated and spring-mounted tail flap was carried out to understand the effect of a tail actuation on the performance of the wing. The front flap actuation, although results in increase in lift-to-drag ratio, is limited in its effectiveness as any leading edge vortex produced has to be convected downstream. This usually results in higher drag. It is hypothesized that a tail flap, however, can help alleviate this, as periodic oscillation of the tail flap may help reduce drag.

Tests were performed to study the effect of a passively actuated tail flap at 0° angle of attack. At this angle of attack, the tail flap was initially perturbed by setting the flap angle at $\theta = 10°$. With the tail flap, positive lift and drag forces (with flap in the downward position) results in anti-clockwise torque and tries to move the flap toward $\theta = 0°$. Likewise, with flap in an upward position, drag and negative lift act to bring the flap in its neutral mean position. The forces acting on the tail flap configuration are thus stabilizing. To obtain large deflections of the flap, the moment-of-inertia ratio was required to be reduced substantially (almost 10 times smaller than the front flap), indicating that a lighter tail is necessary. At zero angle of attack, the tail flap exhibits periodic oscillations around $\theta = 0°$, but the oscillations damp (even with $\xi = 0$), confirming the stabilizing effect of the net flow-induced torque on the tail flap.

A range of studies were conducted at $Re = 14700$ and $\alpha = 10°$ and different spring constants. The flap moment-of-inertial ratio was fixed at $\mathcal{I}^* = 8.4$, an order of magnitude smaller than the front flap computations. For the tail flap, the mean flap angle desired is $\theta = 0°$. The flow induced tail-flap oscillations for the cases studied resulted in small oscillations in the tail and almost an increase of around 10% in lift-to-drag ratio as shown in table 2.

Table 2: Passive actuation of tail flap at $\alpha_0 = 10°$, $Re_c = 14700$, $I^* = 8.4$, $\xi = 0$.

$\mathrm{St_N} = \mathrm{f_N}\ell_\mathrm{a}/\mathrm{U}_\infty$	$\bar{C}_D$	$\bar{C}_L$	$\bar{C}_L/\bar{C}_D$
∞ (no actuation)	0.219	1.039	4.74
0.16	0.22	1.141	5.15
0.55	0.244	1.22	4.98

3.4 Flow Over a Plunging Thin Flat Airfoil with Passively Actuated Tail Flap

With actuated tail flap at 10°, oscillations in the flap angle were observed around the mean position; however, the oscillations were not consistently periodic at least for the cases studied. Subsequently, it was conjectured that, tail flap may be very effective in cases related to flapping wing design, wherein the airfoil is undergoing some combination of plunging/pitching motion, thus resulting in periodic variations in drag and lift forces on the entire wing as well as the tail flap. It was hypothesized that a torsion spring mounted tail flap

and ensuing flexibility of the tail may result in periodic flapping of the tail to reduce drag and/or result in increased thrust.

Accordingly, simulations were performed on a plunging, thin flat airfoil (representative of flapping wing) with a torsion-spring mounted, passively actuated tail flap. Plunging together with flap flexibility adds considerable parameters to the problem; for example, plunging amplitude ($h = a_{\mathrm{LE}}/c$, where a_{LE} is the leading edge amplitude, c is the chord length), plunging reduced frequency ($k = \frac{\pi f c}{U_\infty}$), angle of attack, and plunging waveform. In addition, all the spring parameters are needed for a passive actuated tail. As the first step, a small parameter space was explored with the angle of attack $\alpha_0 = 5^\circ$, plunging amplitude $h = 0.05$, and reduced frequency $k = 5.71$ (10 Hz). The spring flexibility was varied by changing the stiffness constant. The natural frequency of the spring was varied over a wide range covering the plunging frequency; $f_{\mathrm{N}} = 0, 5, 8, 10, 12.5, 20$ Hz. The damping parameter was held fixed at $\xi = 0.01$ for all cases. The tail flap moment-of-inertia ratio is assumed to be $\mathcal{I}^* = 8.4$ and the flow Reynolds number is 14700. The mean flap angle is assumed to be zero (i.e. $\theta_{\mathrm{offset}} = 0$) (refer to Figure 1).

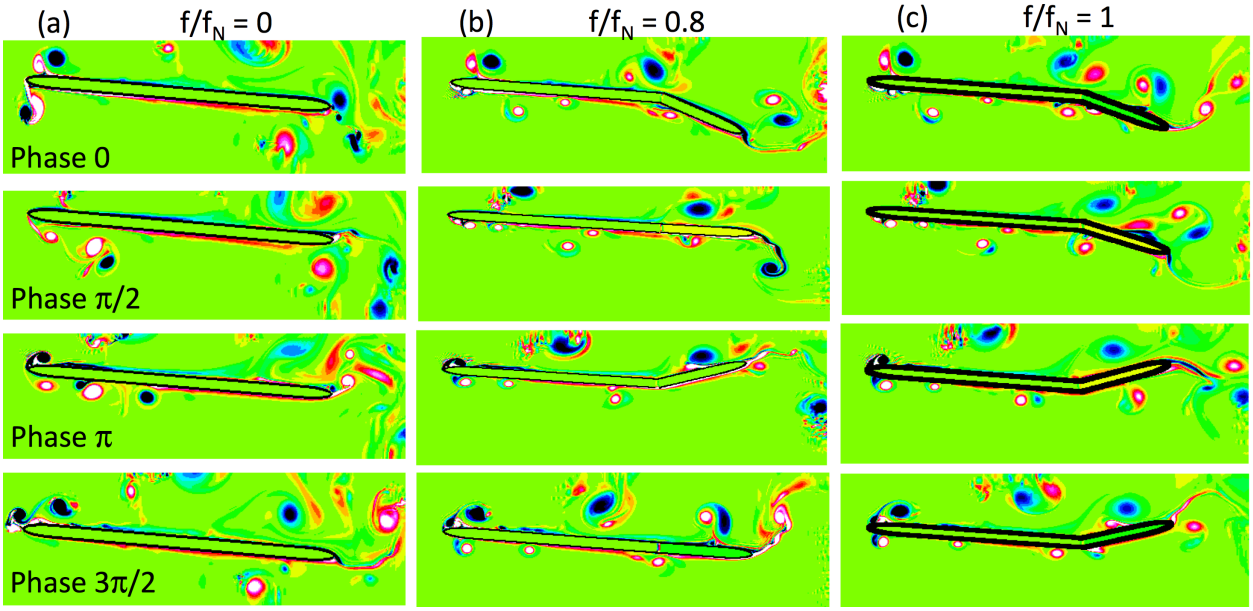

Figure 7: Temporal out-of-plane vorticity contours for one period of plunging motion, $Re = 14700$, $h/c = 0.05$, $f = 10$ Hz: (a) $f/f_{\mathrm{N}} = 0$ (no actuation); (b) $f/f_{\mathrm{N}} = 0.8$, and (c) $f/f_{\mathrm{N}} = 1$. Phase 0 is the center position going up, phase $\pi/2$ is top-most position, phase π is center position going down, and phase $3\pi/2$ is bottom most position.

With the above parameters, a plunging airfoil without any tail actuation (i.e. stiff spring or $f_{\mathrm{N}} = \infty$), the airfoil results in a small mean drag; $\bar{C}_D = 0.0164$ with a mean lift coefficient of $\bar{C}_L = 0.645$. The amplitude of plunging oscillation to the thickness of the airfoil $a_{\mathrm{LE}}/t_a = 0.128$ is much smaller for this thin flat airfoil compared to the standard plunging case using the SD7003 airfoil [26, 18, 18] ($a_{\mathrm{LE}}/t = 0.58$) that results in thrust. Thus, to obtain thrust from pure plunging oscillations, the amplitude of the oscillation would have

to be increased. This small amplitude was chosen to see if it is possible to obtain thrust for the airfoil using passive actuation, providing substantial gain in performance compared to plunging without oscillations. The plunging oscillation was a simple sinusoidal oscillation given as, $h(t) = a_{\mathrm{LE}}\sin[2kt]$. More than 10 complete cycles of plunging were computed before the passive actuation was initiated.

Figure 7 shows the out-of-plane vorticity contours for four different phases for a single plunging cycle for $f/f_{\mathrm{N}} = 0$ (no actuation), $0.8, 1$. The plots show positions of the trailing edge tip with passive actuation compared to the corresponding positions with simple plunging motion. For $f/f_{\mathrm{N}} = 0.8$, starting with phase 0 (center position of the airfoil), the trailing edge is at its lowest downward position. From phase 0 to $\pi/2$, the leading edge is rising upward and reaches the top most position at phase $\pi/2$. The trailing edge, starting from its lowest position also rises upwards (rotates counter-clockwise) and is perfectly aligned with the leading edge at the top-most position. Between phase $\pi/2$ to π, the leading edge starts its downward motion, whereas the trailing edge is still rising (rotating counter-clockwise). Starting from phase π (the center position), the leading edge continues to move downward and reaches its lowest point at $3\pi/2$. Between this section, the trailing edge also starts its downward motion (rotates clock-wise) and aligns perfectly with the leading edge at $3\pi/2$. There exists a phase difference of exactly $\pi/2$ between the leading and trailing edge motions at this spring flexibility. Similar events can be traced for $f/f_{\mathrm{N}} = 1$, however, the phase difference is less than $\pi/2$. At this flexibility, the trailing edge traverses the most distance (largest amplitude variation), owing resonance due to matching of the forcing and spring natural frequencies.

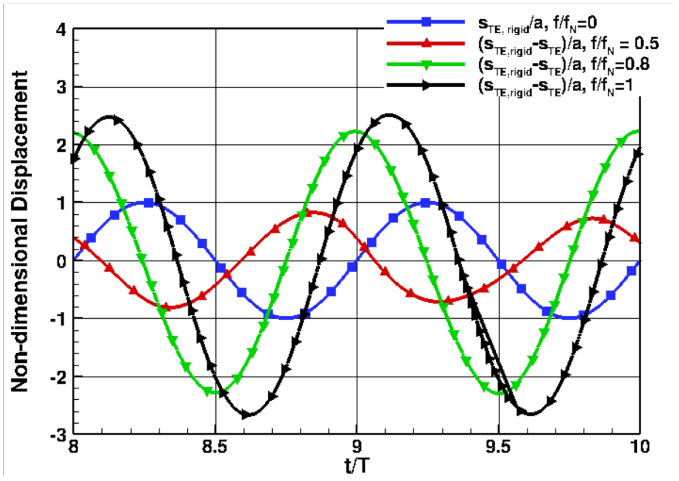

Figure 8: Non-dimensionlized relative motion of the leading and trailing edge tips for various flexibility level of the torsion spring. Also shown is the sinusoidal signal of leading edge motion (blue line); $Re = 14700$, $h/c = 0.05$, $f = 10$ Hz.

To explain these observations, the amplitudes and phase of trailing edge motion relative to the leading edge were examined. Figure 8 shows the time signal of the $(s_{\mathrm{TE,rigid}} - s_{\mathrm{TE}})/a_{\mathrm{LE}}$ over two cycles of plunging motion for four cases $f/f_{\mathrm{N}} = 0, 0.5, 0.8, 1$. Also shown is the signal for a rigid tail (no actuation), which is simply the sine wave. The positive peak of the sine wave represents top most position of the trailing edge whereas the negative peak is the bottom most position. It is observed that the resonant frequency case ($f/f_{\mathrm{N}} = 1$) results in the largest amplitude as expected. For $f/f_{\mathrm{N}} = 0.8$, the trailing edge tip is 90° out of

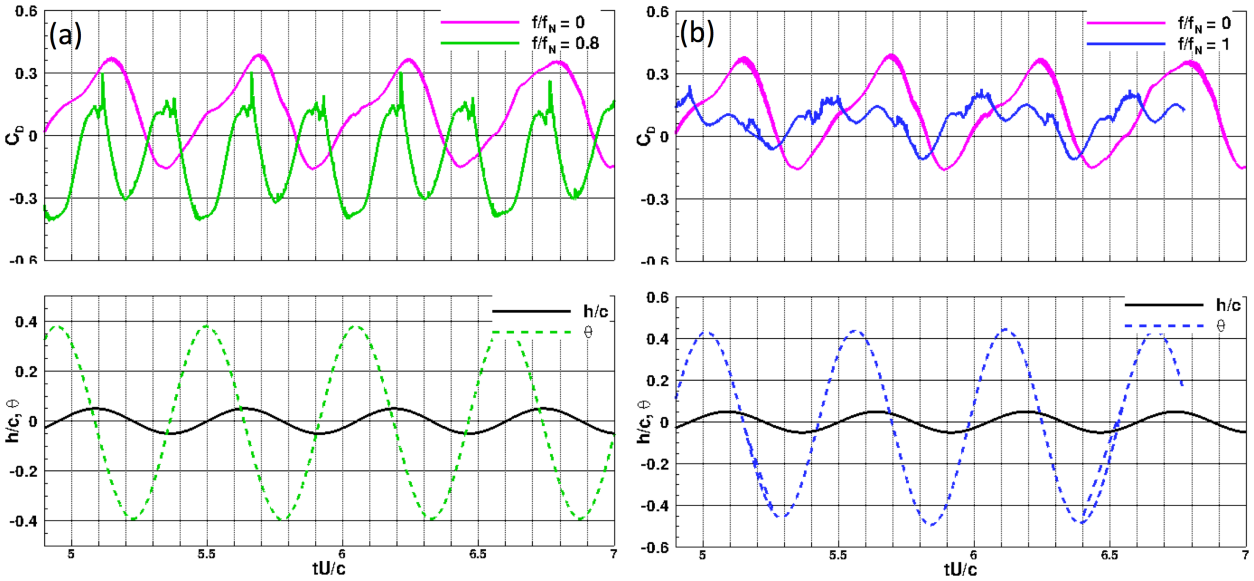

Figure 9: Temporal variation of drag coefficient of the trailing edge flap and flap angle over few cycles of plunging motion, $Re = 14700$, $h/c = 0.05$, $f = 10$ Hz: (a) $C_{D,\text{flap}}$ and θ for $f/f_\text{N} = 0.8$; (b) $C_{D,\text{flap}}$ and θ for $f/f_\text{N} = 1$. Also shown is the drag coefficient for no actuation case ($f/f_\text{N} = 0$) and the sinusoidal motion of the leading edge.

phase of the leading edge. Figure 9 shows the time evolution of the drag coefficient on the tail flap over few periods of oscillation for $f/f_\text{N} = 0.8$ and $f/f_\text{N} = 1$ compared with $f/f_\text{N} = 0$ (i.e. no actuation). Starting with the sinusoidal signal ($h/c = 0$ and increasing sine signal), four different phases are compared (also refer to figure 7):

- Phase 0: At this point, the leading edge is at its center position and is rising up. It is observed that the trailing edge flap has the maximum positive θ for $f/f_\text{N} = 0.8$ (i.e. the trailing edge tip is below the corresponding tip for no-actuation case) and corresponding negative $C_{D,\text{flap}}$. For no actuation (or rigid tail), the drag coefficient at this position is nearly zero. For $f/f_\text{N} = 1$, the flap angle is positive but lower than its maximum value, whereas the drag coefficient is positive.
- Phase $\pi/2$, (maximum positive h/c): At this point, the trailing edge has reached its top-most position and getting ready to start moving downwards. It is observed that for $f/f_\text{N} = 0.8$, the flap angle is decreasing and reached $\theta = 0$, i.e. trailing edge moved upward and is coinciding with the trailing edge of a non-actuated flap. At this stage there is small positive drag on the tail flap. For $f/f_\text{N} = 1$, the trailing edge is still moving upwards but is below the corresponding rigid airfoil edge. This also results in positive drag.
- Phase π: At this point, the trailing edge has reached its center position again and getting ready to start moving further downward. It is observed that for $f/f_\text{N} = 0.8$, the flap angle has reached its highest negative value, i.e. trailing edge continued to move upward and is now further up compared to the trailing edge of a non-actuated flap. At this stage there is again negative drag (thrust). For

$f/f_{\rm N} = 1$, the trailing edge is also moving upwards and a negative drag (thrust) is obtained.

- Phase $3\pi/2$: At this point, the trailing edge has reached its lowest position and getting ready to start moving upward. It is observed that for $f/f_{\rm N} = 0.8$, the flap angle is zero, i.e. trailing edge continued to move downward and is now coinciding with the trailing edge of a non-actuated flap. At this stage there is again small positive drag. For $f/f_{\rm N} = 1$, the trailing edge is moving downwards and still above the trailing edge without no actuation. This also results in positive drag.

The four phases of the airfoil cycle indicate that, for $f/f_{\rm N} = 0.8$, the tail flap adds an additional kicking motion that results in displacing the fluid away from the airfoil in such a way that the cumulative effect together with plunging motion is decrease in net drag or a resultant thrust on the airfoil. The case with $f/f_{\rm N} = 1$ tries to have the same effect, but lags in its position of the trailing edge tip and results in net positive drag.

Table 3 lists the effect of increased flexibility of the torsion spring and passive actuation of the tail on the drag and lift coefficients, as well as the propulsion efficiency. The propulsion efficiency is defined as:

$$\eta = -\frac{\overline{F}_D U_\infty}{\overline{F_L v}} = -\frac{\overline{C_D}}{\overline{C}_{\rm prop}}; \quad \overline{C}_{\rm prop} = \frac{\overline{F_L v}}{\frac{1}{2}\rho U_\infty^3 c}, \tag{4}$$

where the negative sign is because the force considered is drag (instead of thrust)and $\overline{C}_{\rm prop}$ is the average power input for the plunging motion. Here, v is the vertical velocity due to plunging motion. The first column $f/f_{\rm N}$ provides the ratio of plunging frequency to the spring natural frequency, starting from 0 (i.e. rigid spring, no actuation) to increasing flexibility. The second column lists the ratio of the amplitude of the leading edge (mainly following the plunging motion) to the trailing edge (consisting of plunging motion together with motion due to actuation of the trailing edge). For $f/f_{\rm N} = 1$, a resonance effect is expected and one obtains the largest variation in the amplitude ratios. Next four columns list the mean drag and lift coefficients on the trailing edge flap and on the entire airfoil, respectively. It is observed that the rigid tail gives small positive mean drag. With passive actuation and increasing flexibility ($f < f_{\rm N}$), mean thrust is obtained, whereas the mean lift coefficient also increases slightly. Further increase in flexibility ($f \geq f_{\rm N}$) shows increase in mean drag on the airfoil. It is also observed that for $f/f_{\rm N} = 0.5$ and 0.8, the tail flap itself produces thrust and resultant thrust for the entire wing is even higher. With further increase in flexibility of the spring, the tail flap actually provides more drag than the overall wing, indicating that with increase in flexibility, the tail moves in a position relative to the wing that results in increased drag on the system. The last column lists the propulsion efficiency. For $f/f_{\rm N} = 0.5$ and 0.8, net positive efficiency (thrust) is obtained for otherwise negative efficiency without any actuation. This result is very encouraging and suggests that there exists a range of flexibility that improves performance of the flapping wing, whereas too much flexibility

can affect the efficiency negatively.

Table 3: Effect of passively actuated tail flap on performance of a plunging foil: $k = \frac{\pi fc}{U_\infty} = 5.71$, (f = 10 Hz) $\alpha_0 = 5°$, $Re_c = 14700$, $I^* = 8.4$, $\xi = 0.01$

f/f_N	a_{TE}/a_{LE}	Flap $\bar{C}_D$	Flap $\bar{C}_L$	$\bar{C}_D$	$\bar{C}_L$	$\bar{C}_{prop}$	η
0 (rigid)	1.0	+0.1103	0.059	+0.0164	0.645	0.556	-0.032
0.5	0.815	-0.014	0.0693	-0.1	0.662	0.83	+0.133
0.8	2.24	-0.11	0.1	-0.162	0.7245	0.729	+0.244
1	2.58	+0.0715	0.13	+0.071	0.65	0.237	-0.33
1.25	2.045	+0.165	-0.067	+0.12	0.044	0.118	-1.18
2	1.245	+0.167	-0.035	+0.122	0.333	0.178	-0.76

4 Summary and Future Work

Effect on airfoil performance due flow-induced passive actuation of a spring-mounted flap (leading and trailing) at low Reynolds number was investigated using two-dimensional DNS studies. The flap, attached with a torsion spring at one-third the chord length, is modeled as a spring-mounted compound pendulum with single-degree of freedom. It may undergo flow induced rotation resulting in dynamic variations in the effective angle of attack as well as the airfoil shape. A second-order, fictitious domain method [28] was further extended to account for flow-structure interaction problems and verified to show good predictive capability, compared to AFRL's flow-structure interaction solver (FDL3DI) [17].

Use of a spring-mounted leading edge flap (at 20° angle of attack and $Re = 14700$) was studied by varying the flap moment-of-inertia (or flap weight) and the spring stiffness parameter (or natural frequency). For the parameters studied, a range of spring natural frequency (around 3 Hz) was identified to provide limit cycle oscillations of the leading edge flap around its mean horizontal position. In this lock-in region, the mean lift-to-drag ratio increased considerably compared to no actuation case. Increase in the flap weight resulted in decreased amplitude of the flap motion and resulted in better mean lift-to-drag ratio. For very heavy flap (or almost static actuator), the leading edge flap underwent almost no oscillation and provided the most increase in lift-to-drag ratio. Use of a spring-mounted trailing edge flap was also studied at 10° angle of attack and $Re = 14700$ at various moment-of-intertia ratios and spring flexibility. The trailing edge flap also resulted in a flow-induced flap oscillation around its mean configuration and an increase in mean lift-to-drag ratio by 10% was observed. The trailing edge flap was observed to be a stabilizing configuration, with drag and lift forces creating torques around the hinge that tries to rotate the flap toward its mean position. On the other hand, with the leading edge flap, the drag and lift forces on the flap result in flap motion away from the desired mean position.

Of particular importance was application of the spring-mounted trailing edge flap concept to a plunging wing. High-frequency, low amplitude plunging wing can be used to approximate wing motion in a flapping wing design. Effect of trailing edge actuation on a plunging thin, flat airfoil (k=5.71, h=0.05) was investigated at 5° angle of attack. For the parameters chosen, without any actuation (extremely stiff spring), the foil resulted in a small positive drag. By introducing some spring flexibility, the drag coefficient decreased and lift coefficient increased showing increase in performance of the wing. For certain spring parameters resulting in spring natural frequencies slightly larger than the plunging frequency ($f/f_{\mathrm{N}} = 0.5-0.8$), dramatic increase in performance was observed. The wing motion resulted in thrust and higher lift coefficients with a propulsive efficiency as high as 24.4%. It was found that most increase in propulsive efficiency was obtained when the trailing edge tip was 90° out-of-phase with the leading edge, an observation consistent with experimental data on plunging teardrop airfoils with flexible tail filament by Heathcote and Gursul [35, 36, 23]. It was also observed that, there exists a range of spring flexibility that results in enhanced performance (increased thrust and/or propulsive efficiency). However, too much flexibility of the spring can adversely affect performance, again a consistent result similar to observations related that of purely flexible trailing edge filament.

This suggests that use of a single-degree of freedom spring-mounted trailing edge flap and resulting passive control can be used as a simplified canonical mechanism to study effect of trailing edge flexibility on flapping wing design. The results are of direct relevance to other forms of flow control which are more amenable to small scale MAV implementation of current interest to AFOSR; for example, surface deformations via piezo-electric actuators or aero-elastically tailored structures. Use of leading and trailing edge flaps (either actively or passively controlled) provide an effective way to increase foil performance and provide means to control the lift and drag characteristics under transient maneuvers or flow disturbances.

The summer research at AFRL's computational sciences division has resulted in several opportunities for future collaborations with AFRL scientists and researchers. At Oregon State, new projects for senior students are initiated to build and modify the existing physical setup and measure lift and drag coefficients. A University Honors College thesis [25], an AIAA conference paper [26] have been completed and couple of students, supported as Teaching Assistants, are working toward their Master's degree on related topics. The current research work will be presented at American Physical Society's Division of Fluid Dynamics Meeting (November 2011) in Baltimore. In addition, we are presently building a physical setup of torsion-spring mounted trailing edge flap for wind-tunnel testing that can be used for wide range of parametric studies.

References

[1] Y. Hoarau, M. Braza, Y. Ventikos, D. Faghani, G. Tzabiras, Organized modes and the three dimensional transition to turbulence in the incompressible flow around a NACA0012 wing, J. Fluid Mech. 496 (2003) 63–72.

[2] H. Nishimura, Y. Taniike, Aerodynamic characteristics of fluctuating forces on a circular cylinder, J. Wind Eng., Ind. Aerodynamics 89 (2001) 713–723.

[3] C. Sicot, S. Auburn, S. Loyer, P. Devinant, Unsteady characteristics of the static stall of an airfoil sujected to freestream turbulence level up to 16%, Exp. in Fluids 41 (2006) 641–648.

[4] A. Fabula, This airfoil theory applied to hydrofoils with a single finite cavity and arbitrary free-streamline detatchment, J. Fluid Mech. 12 (1962) 227–240.

[5] H. Kao, Some aspects of airfoil stall in low speed flow, J. Aircraft 11 (3) (1974) 177–180.

[6] T. Mueller, J. DeLaurier, An overview of micro air vehicle aerodynamics.' Fixed and flapping wing aerodynamics for micro air vehicle applications, Progress in Astronautics and Aeronautics 195 (2001) 1–10.

[7] A. Pelletier, T. Mueller, Low Reynolds number aerodynamics of low-aspect ratio, thin/flat/cambered-plate wings, J. of Aircraft 37 (5) (2000) 825–832.

[8] A. Broeren, M. Bragg, Unsteady stalling characteristics of thin airfoils at low Reynolds numbers. Fixed and flapping wing aerodynamics for micro air vehicle applications, Progress in Astronautics and Aeronautics 195 (2001) 191–213.

[9] S. Brunton, C. Rowley, K. Taira, T. Colonius, J. Collins, D. Williams, Unsteady aerodynamic forces on small-scale wings: experiments, simulations and models, in: 46 th AIAA Aerospace Sciences Meeting and Exhibit, American Institute of Aeronautics and Astronautics, 1801 Alexander Bell Drive, Suite 500, Reston, VA, 20191-4344, USA,, 2008.

[10] W. Geissler, H. Sobieczky, H. Vollmers, Numerical study of the unsteady flow on a pitching airfoil with oscillating flap, in: European Rotorcraft Forum, 24 th, Marseilles, France, 1998.

[11] Y. Lu, G. Shen, G. Lai, Dual leading-edge vortices on flapping wings, Journal of Experimental Biology 209 (24) (2006) 5005.

[12] F. Muijres, L. Johansson, R. Barfield, M. Wolf, G. Spedding, A. Hedenstrom, Leading-edge vortex improves lift in slow-flying bats, Science 319 (5867) (2008) 1250.

[13] M. Dickinson, F. Lehmann, S. Sane, Wing rotation and the aerodynamic basis of insect flight, Science 284 (5422) (1999) 1954.

[14] K. Taira, W. Dickson, T. Colonius, M. Dickinson, C. Rowley, Unsteadiness in flow over a flat plate at angle-of-attack at low Reynolds numbers, in: 45 th Aerospace Sciences Meeting and Exhibit, AIAA,(AIAA 2007-710).

[15] K. Taira, T. Colonius, Three-dimensional flows around low-aspect-ratio flat-plate wings at low Reynolds numbers, Journal of Fluid Mechanics 623.

[16] T. Colonius, C. Rowley, G. Tadmor, D. Williams, K. Taira, W. Dickson, M. Gharib, M. Dickinson, Closed-loop control of leading-edge and tip vortices for small UAV, in: Conference on Active Flow Control, 2006.

[17] M. Visbal, High-fidelity simulation of transitional flows past a plunging airfoil, AIAA paper 391 (2009) 2009.

[18] M. Visbal, R. Gordnier, M. Galbraith, High-fidelity simulations of moving and flexible airfoils at low Reynolds numbers, Experiments in Fluids 46 (5) (2009) 903–922.

[19] W. Shyy, M. Berg, D. Ljungqvist, Flapping and flexible wings for biological and micro air vehicles, Progress in Aerospace Sciences 35 (5) (1999) 455–505.

[20] S. Ho, H. Nassef, N. Pornsinsirirak, Y. Tai, C. Ho, Unsteady aerodynamics and flow control for flapping wing flyers, Progress in Aerospace Sciences 39 (8) (2003) 635–681.

[21] K. Jones, M. Platzer, Design and development considerations for biologically inspired flapping-wing micro air vehicles, Experiments in fluids 46 (5) (2009) 799–810.

[22] M. Triantafyllou, G. Triantafyllou, D. Yue, Hydrodynamics of fishlike swimming, Annual review of fluid mechanics 32 (1) (2000) 33–53.

[23] S. Heathcote, Z. Wang, I. Gursul, Effect of spanwise flexibility on flapping wing propulsion, Journal of Fluids and Structures 24 (2) (2008) 183–199.

[24] S. Apte, DNS of low Reynolds number flow dynamics of a thin airfoil with an actuated leading, ASEE SFFP Final Report, Wright Patterson Airforce Base (2010) http://web.engr.oregonstate.edu/ sva/reports.html.

[25] K. Drost, Direct Numerical Simulation of a Flat Wing with a Movable Front Flap at High Angles of Attack and Low Reynolds Numbers, University Honors College B.S. Thesis, Oregon State University.

[26] K. Drost, H. Johnson, S. Apte, J. Liburdy, Low Reynolds number flow dynamics of a thin airfoil with an actuated leading edge, in: AIAA-2011-3944, 41st AIAA Fluid Dynamics Conference, American Institute of Aeronautics and Astronautics, Honolulu, HI, USA, 2011.

[27] S. Scott Collis, R. Joslin, A. Seifert, V. Theofilis, Issues in active flow control: theory, control, simulation, and experiment, Progress in Aerospace Sciences 40 (4-5) (2004) 237–289.

[28] S. Apte, M. Martin, N. Patankar, A numerical method for fully resolved simulation (FRS) of rigid particle-flow interactions in complex flows, Journal of Computational Physics (2008) doi:10.1016/j.jcp.2008.11.034.

[29] S. Apte, J. Finn, A variable density fictitious domain method for fully resolved simulation of high-density ratio fluid-particle systems, in: ICMF2010, Seventh International Conference on Multiphase Flow, Tampa Bay, FL.

[30] P. Moin, S. Apte, Large eddy simulation of multiphase reacting flows in complex combustors, AIAA J. (special issue on 'Combustion Modeling and LES: Development and Validation Needs for Gas Turbine Combustors) 44 (2006) 698–710.

[31] S. Morton, R. Melville, M. Visbal, Accuracy and coupling issues of aeroelastic navier-stokes solutions on deforming meshes, Journal of aircraft 35 (5) (1998) 798–805.

[32] H. Blackburn, G. Karniadakis, Two-and three-dimensional simulations of vortex-induced vibration of a circular cylinder, in: Proceedings of the Third International offshore and polar engineering conference, Citeseer, 1993.

[33] J. Yang, S. Preidikman, E. Balaras, A strongly coupled, embedded-boundary method for fluid-structure interactions of elastically mounted rigid bodies, Journal of Fluids and Structures 24 (2) (2008) 167–182.

[34] D. Kim, H. Choi, Immersed boundary method for flow around an arbitrarily moving body, Journal of Computational Physics 212 (2) (2006) 662–680.

[35] S. Heathcote, I. Gursul, Jet switching phenomenon for a periodically plunging airfoil, Physics of Fluids 19 (2007) 027104.

[36] S. Heathcote, D. Martin, I. Gursul, Flexible flapping airfoil propulsion at zero freestream velocity, AIAA journal 42 (11).